Toward a dynamic model for the near-wall region based on reduced representations

By T. Sayadi†, P. J. Schmid‡, C. W. Hamman AND A. Lozano-Durán

As a continuation of previous efforts (partly conducted during the CTR Summer Program in 2014), the near-wall region of a weakly compressible boundary layer will be studied. Reduced-order representations based on the Dynamic Mode Decomposition (DMD) will be coupled with sparsity-promoting system identification techniques to arrive at a low-dimensional dynamic representation of the near-wall dynamics. Particular emphasis will be put on the feasibility of a localized identification of a reduced-order model that can be globally applied over the spatial extent of a transitioning boundary layer. The recently developed parallel DMD algorithm will facilitate this type of analysis. In a second step, a driven state-space model is derived from the identified structures, and a transfer function between coherent velocity input and coherent stress output in a user-specified wall-parallel plane is constructed. This transfer function acts as a map between resolved velocity fields (from Large-Eddy Simulations, LES) and resolved stress components (entering the subgrid-scale model) and is intended to alleviate the resolution requirements of wall-resolved LES.

1. Motivation and background

LES constitute an important tool in the study of turbulent fluid flows at Reynolds numbers that approach values found in technological and industrial applications. Only large-scale structures are resolved; smaller scales that can no longer be resolved by the chosen grid are modeled, and their effect on the resolved scales is accounted for by a subgrid-scale model. Near the walls, where smaller scales prevail, resolution requirements of wall-resolved LES approach those of direct numerical simulations (DNS). This restriction severely limits the applicability of LES in the high-Reynolds-number flows and complex geometries that are typically of engineering interest. To overcome this computational bottle-neck, an alternative solution technique consists of a wall-modeled simulation, where the perturbation dynamics close to the wall is replaced by a representative reduced-order model that provides information to the outer flow and thus removes numerical stiffness. These models typically provide shear stress information that is fed to the outer flow in the form of an inhomogeneous or dynamic boundary condition. Previous and recent investigations concerned with the design of proper wall models have used turbulent scaling laws, control-theoretic approaches or neural-network techniques, to name but a few, in an attempt to arrive at an approximate but sufficiently accurate representation of the fluid flow in the vicinity of the wall.

In a previous study Sayadi & Schmid (2014) applied the DMD formalism to the DNS data of a turbulent boundary layer. This study showed that using merely two low-frequency DMD modes produces an acceptable representation of the motion of coherent structures close to the wall. The selected modes from this earlier example, however,

† RWTH Aachen University, Germany
‡ Imperial College London, U.K.

are weakly dependent on (i) the location of the subdomain from which they have been sampled and (ii) the number of snapshots used to decompose the data. In a subsequent investigation (Sayadi & Schmid 2016), a parallelized and highly scalable DMD algorithm has been developed and applied to decompose the transitional dataset (Sayadi *et al.* 2013) in its entirety, i.e., capturing simultaneously the laminar, transitional and fully turbulent regime. In contrast to the transitional regime, where the processed flow fields are periodic in time, the turbulent regime is characterized by non-periodic motion (with an associated broadband spectrum) and a break in spanwise symmetry. From the modal shape of the subdomain analysis, it can be deduced that the length of the streaky structures is larger than the streamwise extent of the identified subdomain, which may be a contributing factor to the mismatch between the reduced-order model and the full Reynolds stress distribution. As an added benefit of the full-domain decomposition, the dependence of the modal shapes on the number of snapshots is greatly reduced, and the modes are conditioned by the dominant harmonic and subharmonic frequencies of the laminar and transitional flows. Analysis of the late transitional regime Sayadi *et al.* (2014) has shown that the same low-frequency modes contribute to most of the shear stress close to the wall and reproduce turbulent statistics similar to that of the fully turbulent regime. However, due to the broadband nature of turbulence, these dominant low-frequency modes are not easily identified using DMD applied only to the turbulent subdomain. This observation highlights the advantage of performing a full-sized decomposition analysis even if the region of interest is localized in the far downstream section.

In this study, we will use the coherent near-wall structures (defined by the organized motion of fluctuating fluid elements and mathematically described by a phase average) together with a triple decomposition of the governing equations to derive and validate a system-theoretic model that describes the response in the coherent part of the Reynolds stresses to a driving by the coherent part of the velocity field. The details of this response behavior are expressed in the form of a transfer function whose gain-structure furnishes important information about the design of low-dimensional impedance boundary conditions for a replacement of the near-wall dynamics by a selectively reflective boundary.

2. Formulation and computational setup

A starting point for the analysis is the triple decomposition of the velocity field, as introduced by Reynolds & Hussain (1972). It decomposes a turbulent flow field $\mathbf{u}$ into a time-averaged part, denoted by $\bar{u}$, a phase-averaged, coherent part, denoted by $\tilde{u}$, and a remaining part consisting of incoherent fluctuations u'.

Applying this approach to the Navier-Stokes equations for incompressible flow with constant material properties, we can derive an evolution equation for the coherent structures (described by $\tilde{u}$). This set of equations, however, is not closed as it is driven by terms of the form $\tilde{r}_{ij} = \langle u_i' u_j' \rangle - \overline{u_i' u_j'}$, which represents the Reynolds shear-stress exerted by the organized motion in the flow. In the above, $\langle \cdot \rangle$ stands for a phase average, while $\bar{\cdot}$ denotes a time average.

An equation of motion for the coherent Reynolds stress components $\tilde{r}_{ij}$ can be derived using standard procedures. In its original form, this equation is rather cumbersome to analyze, and further simplifications for our special case of near-wall motion are necessary to arrive at a more tractable equation.

To this end, we combine the nonlinear terms as well as the unclosed triple moments into a driving term on the right-hand side of an otherwise linear evolution equation for

$\tilde{r}_{ij}$. Furthermore, since we are mostly interested in the response to coherent driving of the stresses by velocities, we will concentrate on the linearized left-hand side of the equation rather than the structure of the right-hand side.

The emphasis on the near-wall region allows further simplification, where a number of gradients and components of the dependent flow quantities are reduced based on dominant balances. Details of this procedure can be found in Schmid & Sayadi (2016). In a final step, the homogeneous wall-parallel coordinate directions are Fourier-transformed, thus introducing a streamwise wavenumber and a spanwise wavenumber, which we denote by α and β, respectively. In addition, we define a wavenumber modulus k as $k^2 = \alpha^2 + \beta^2$. The dependence on the wall-normal coordinate direction y remains, and differentiation with respect to y is given by symbol d.

Our main concern is the derivation of a reflective boundary condition implemented at a selected wall-parallel distance that supplies a coherent Reynolds stress behavior given an extracted coherent velocity field. For this reason, we concentrate on a linearized evolution equation for the Reynolds stress components of the form

$$\frac{\partial}{\partial t}\mathbf{R} = \mathsf{D}\mathbf{R} + \mathsf{C}\mathbf{U}, \tag{2.1}$$

which constitutes a driven linear system, with the coherent velocity fields, summarized in $\mathbf{U}$, as input and the coherent Reynolds stress components, denoted by $\mathbf{R}$. The state matrices C, D are given – under the above assumptions – as

$$\mathsf{C} = \begin{pmatrix} 2i\alpha\overline{u'u'} + 2\overline{u'v'}d & \overline{u'u'}_{,y} & 0 \\ 0 & \overline{v'v'}_{,y} + 2i\alpha\overline{u'v'} + 2\overline{v'v'}d & 0 \\ 0 & \overline{w'w'}_{,y} & i\beta\overline{w'w'} \\ i\alpha\overline{u'v'} + \overline{v'v'}d & \overline{u'v'}_{,y} + i\alpha\overline{u'u'} + \overline{u'v'}d & 0 \\ i\beta\overline{w'w'} & 0 & i\alpha\overline{u'u'} + \overline{u'v'}d \\ 0 & i\beta\overline{w'w'} & i\alpha\overline{u'v'} + \overline{v'v'}d \end{pmatrix} \tag{2.2}$$

$$\mathsf{D} = (i\alpha\bar{u} - \frac{1}{\mathrm{Re}}(d^2 - k^2)) \otimes \mathsf{I}^{6\times 6} - \begin{pmatrix} 0 & 0 & 0 & 2\bar{u}_{,y} & 0 & 0 \\ 0 & 0 & 0 & 0 & 0 & 0 \\ 0 & 0 & 0 & 0 & 0 & 0 \\ 0 & \bar{u}_{,y} & 0 & 0 & 0 & 0 \\ 0 & 0 & 0 & 0 & 0 & \bar{u}_{,y} \\ 0 & 0 & 0 & 0 & 0 & 0 \end{pmatrix}, \tag{2.3}$$

and the state vectors $\mathbf{U}$ and $\mathbf{R}$ are defined as

$$\mathbf{U} = \begin{pmatrix} \hat{\tilde{u}} \\ \hat{\tilde{v}} \\ \hat{\tilde{w}} \end{pmatrix} \qquad \text{and} \qquad \mathbf{R} = \begin{pmatrix} \hat{\tilde{r}}_{uu} \\ \hat{\tilde{r}}_{vv} \\ \hat{\tilde{r}}_{ww} \\ \hat{\tilde{r}}_{uv} \\ \hat{\tilde{r}}_{uw} \\ \hat{\tilde{r}}_{vw} \end{pmatrix}. \tag{2.4}$$

The symbol $\otimes$ stands for the Kronecker product.

While the entries in the system matrix D, governing the dynamics of the Reynolds stress components, only contain the mean velocity profile and its derivatives, the driving matrix C depends on time averages over turbulent fluctuations. This closure problem will be addressed by the triple decomposition and requires an extraction of the respective

matrix entries from a numerical database; this latter step will be accomplished by a DMD of a compressible turbulent boundary layer (Sayadi 2012).

As a database, we use simulations of a compressible ($Ma = 0.2$) boundary layer undergoing H-type transition. The relatively low Mach number ensures that compressibility effects are negligible (which have been verified by comparing incompressible and DNS-based growth rates) and that a model description based on incompressible governing equations is suitable. The simulations were performed over a spatial domain of $L_x \times L_y \times L_z = 9.6 \times 1.0 \times 0.60$ with a spatial resolution of $N_x \times N_y \times N_z = 4096 \times 550 \times 512$, which results in a resolution (in wall units) of $\Delta x^+ \times \Delta y^+ \times \Delta z^+ = 10 \times 0.4 \times 5.4$. The inlet Reynolds number based on the distance from the leading edge is $Re_x = 10^5$. The distance of the inlet from the leading edge is denoted by x_0 and is used as the characteristic lengthscale. Periodic boundary conditions are used in the streamwise and spanwise coordinate directions, and a sponge layer is added to the downstream domain edge to allow for spatial growth of the boundary layer. Inside the sponge layer, fluctuations are damped and a similarity solution of the compressible laminar boundary layer is forced.

3. Setup of the dynamical model

Following the triple decomposition, the near-wall coherent structures can be thought of as the phase-averaged part of the full flow fields (Jeong *et al.* 1997). This phase average will be replaced by the principal structures from a DMD (see Schmid (2010); Schmid *et al.* (2012); Rowley *et al.* (2009); Chen *et al.* (2012); Mezic (2005)). In other words, the contribution of each extracted dynamic mode to the Reynolds shear stress budget is equivalent to the contribution of coherent motion from a specific phase-averaged structure.

More specifically, the DMD processes a data matrix consisting of the velocity components of the flow within the entire computational domain, covering the pre-transitional to the fully developed turbulent regimes, with the Reynolds number Re_θ ranging from 200 to 1410. Each snapshot extracts flow information between the wall and a wall-normal distance of $y^+ = 140$. The parallel version of the DMD (see Sayadi & Schmid (2016)) had to be employed, owing to the exceedingly large number of degrees of freedom. In addition, in order to isolate relevant structures (over the course of the sampling period) from transient but artificial processes, sparsity promotion in the amplitude calculation has been applied according to the algorithm proposed in Jovanovic *et al.* (2014).

Figure 1 shows the DMD spectrum as well as the amplitude distribution versus the extracted frequencies. The two low-frequency modes, identified by the sparsity-promoting algorithm, are indicated by full symbols; their frequencies are $\omega = 0.066$ and $\omega = 0.1222$. Focusing on these two most dominant structures, the flow field can be reconstructed as a superposition of the modal spatial structures, the temporal frequencies and the complex amplitudes (which contain phase information). Figure 2 presents snapshots of the reconstructed flow field, visualized in the entire computational domain by the three velocity components. A clear breakdown of spatial scales across the transition region is visible: coherent instability waves in the laminar region develop a typical secondary instability (with a spanwise symmetry) which subsequently strengthens in the transitional regime and finally triggers the breakdown into turbulent fluid motion and the loss of spanwise symmetry. Each part of this dynamic process is well captured by two dynamic modes that have compact support over the entire computational domain. Despite the eventual breakdown into turbulence, the prevalence of streamwise elongated structures can be observed and quantitatively corroborated.

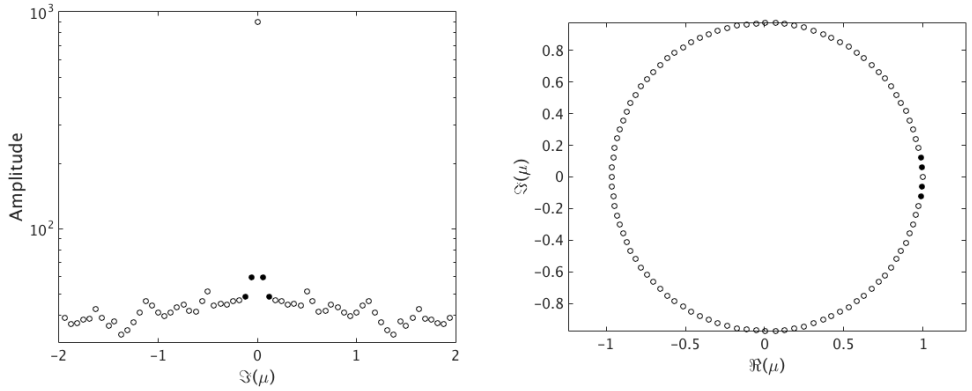

(a) Spectra (b) Eigenvalues, μ

FIGURE 1: Eigenvalue and spectra of the DMD modes for the whole-domain analysis. The two low-frequency modes are highlighted using filled symbols.

With the phase-averaged part of the fluid motion described by two dynamic modes, we are now in a position to determine the statistical quantities that appear as entries in the C-matrix of our above dynamical model. In particular, we use the relation

$$\overline{uu} - \bar{u}^2 = \overline{\tilde{u}\tilde{u}} - \overline{u'u'}. \tag{3.1}$$

The remaining quantities are determined analogously. In the above expression, the fluctuation covariances can be computed knowing the time-averaged and coherent perturbation dynamics.

It is interesting to evaluate the accuracy of the reconstruction in the three identified domains (laminar, transitional and turbulent). Figure 3 compares the streamwise part of the reconstructed coherent motion (using two low-frequency dynamic modes) to the full DNS data. We observe a good agreement between the two datasets throughout the three flow regimes.

4. Analysis of the dynamical model

With all entries in the system matrices C and D determined, we proceed by analyzing the response behavior of the dynamical model to harmonic forcing. This frequency-response analysis provides valuable information about Reynolds stress structures that are particularly responsive to forcing by the coherent velocity elements and structures that are impervious to harmonic excitation. The same information can equally build the foundation for the analysis of near-wall dynamics and for the design of a low-dimensional representation. From a mathematical point of view, the frequency response analysis determines the filter properties of a wall-parallel plane in transferring coherent velocity information into coherent stress information.

The maximum frequency response of our linear model to time-harmonic forcing in $\mathbf{U}$ evaluated in a wall-parallel plane can be cast as

$$R = \max_{\omega} \left\| \mathsf{P}_{\text{out}} (i\omega \mathsf{I} + \mathsf{D})^{-1} \mathsf{C} \mathsf{P}_{\text{in}} \right\|, \tag{4.1}$$

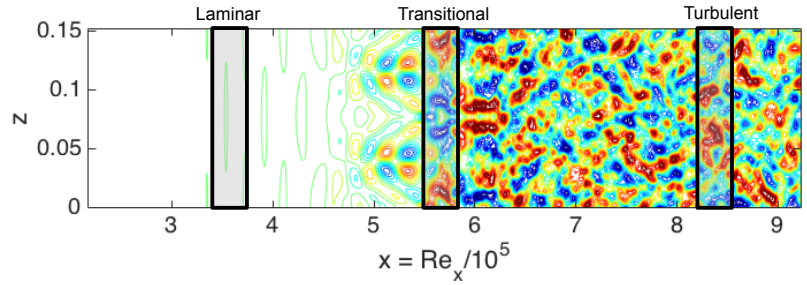

(a) streamwise velocity

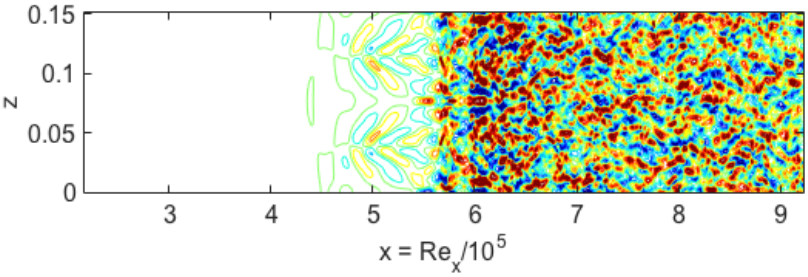

(b) wall-normal velocity

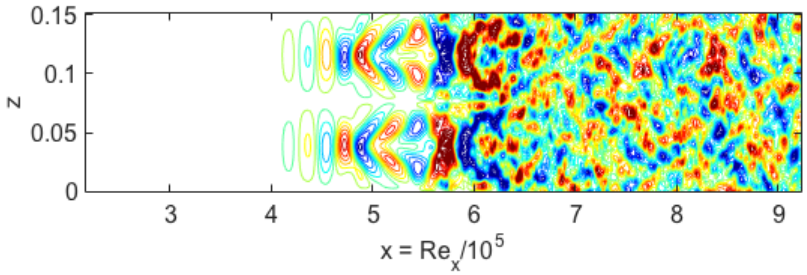

(c) spanwise velocity

FIGURE 2: Reconstructed velocity fields using the two low-frequency modes, visualized in the wall-parallel x-z-plane at $y^+ = 25$. The laminar, transitional and turbulent areas selected for further analysis (see text) are highlighted in (a).

where ω denotes the forcing frequency and $\mathsf{P}_{\text{in}}, \mathsf{P}_{\text{out}}$ stand for matrices that select and restrict the input/output variables. These latter matrices have been chosen to account for a given velocity forcing and stress response only in a user-specified wall-normal plane. By scanning over all forcing-response combinations, we can assess the importance of input-output pairs that yield the largest gain. This analysis (performed for a wall-parallel plane located at $y^+ = 25$ and a forcing frequency of $\omega = 0.066$) revealed that the largest gain results from a forcing of the $\tilde{r}_{uu}$-component by a wall-normal velocity structure $\tilde{v}$. We will thus focus on this input-output pair and further probe the preferred structure responsible for the link between velocity input and Reynolds stress output. The maximum

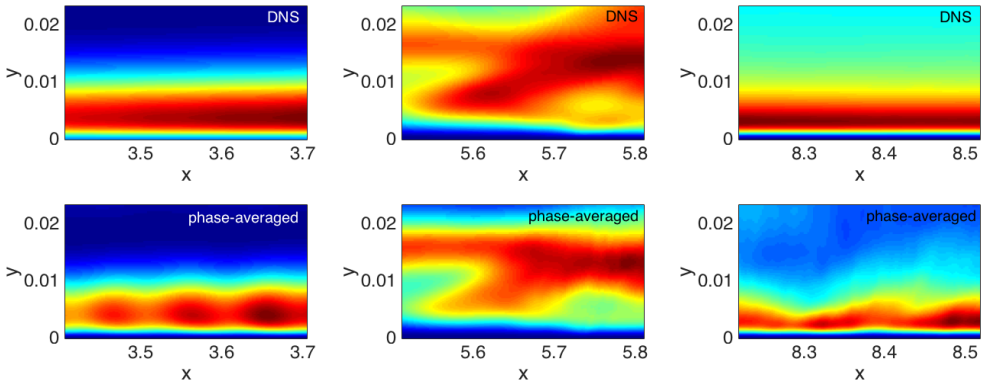

(a) laminar (b) transitional (c) turbulent

FIGURE 3: Comparison of the phase-averaged and the total streamwise fluctuation data in three different regimes of laminar, transitional and turbulent flow, as highlighted in the boxed areas of Figure 2(a).

gain is still dependent on the wall-parallel wavenumbers, i.e., the streamwise and spanwise wavenumbers α and β, respectively.

The norm of the in-plane $\tilde{v} \rightarrow \tilde{r}_{uu}$-transfer function, weighted by the wavenumbers, i.e., $\alpha\beta\|\mathsf{P}_{\text{out}}(i\omega\mathsf{I} - \mathsf{D})^{-1}\mathsf{C}\mathsf{P}_{\text{in}}\|$, is shown in Figure 4. It is characterized by a prominent peak in the α-β-plane, indicating that streamwise elongated Reynolds stress elements are strongly amplified by harmonic velocity input. The spatial aspect ratio, extracted from the peak location, is about 50. This preference for elongated structures has also been observed for other frequencies.

The frequency response as displayed in Figure 4 constitutes a mapping between the coherent velocity field in the wall-parallel plane $y^+ = 25$ and the coherent Reynolds stress tensor components. For a practical implementation, the LES would provide the velocity field, while the resulting stress tensor components would be incorporated into the subgrid-scale model. In this manner, we can replace the dynamics of coherent wall structures by an equivalent reflective boundary condition in the wall-parallel plane. The resolution restrictions stemming from the near-wall region would thus be alleviated.

While preliminary studies on the influence of the chosen plane location (in our case at $y^+ = 25$) on the frequency response behavior have shown a substantial robustness regarding the most amplified structures, a more careful investigation is planned to quantify the accuracy of the reconstructed near-wall motion by an input-output map in a wall-parallel plane and to relate this behavior to physical quantities of the mean profile and the coherent wall structures.

5. Conclusions and outlook

Based on the computational and experimental observation that the near-wall region in turbulent flows can be described by a low-dimensional, reduced-order model that tracks a limited number of coherent structures, we have followed a system-theoretic approach and derived a state-space model that establishes a dynamic link between the coherent

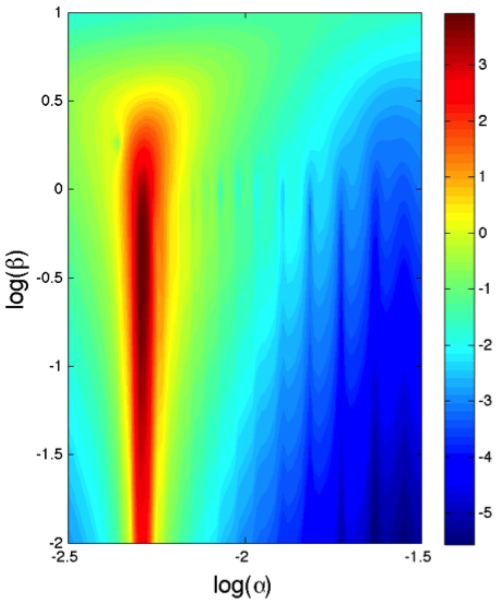

FIGURE 4: Wavenumber-corrected norm of the transfer function describing the mapping of the coherent normal velocity $\hat{\tilde{v}}$ to the coherent stress component $\hat{\tilde{r}}_{uu}$ in the wall-parallel input-output plane at $y^+ = 25$. The transfer function has been evaluated for $\omega = 0.066$, the dominant frequency extracted by DMD from the numerical simulation. The contours are plotted logarithmically.

part of the velocity field and the coherent part of the Reynolds stress components. A triple decomposition of the flow field into time-averaged, phase-averaged and incoherent motion yielded a driven linear system that could be further simplified using common boundary-layer-type scaling assumptions. The entries of the system matrices could be determined from a DMD of the full flow field, followed by a two-mode representation of the phase-averaged near-wall dynamics. The final model has been subjected to a frequency response, evaluated for harmonic velocity input and stress output in a wall-parallel plane located at $y^+ = 25$. A marked peak in gain has been observed for structures that are elongated in the streamwise direction with a spatial aspect ratio of about 50. Moreover, distinct preferences for input-output pairs have been observed, only one of which has been analyzed in this report.

The in-plane transfer function can be implemented as a reflective boundary condition, converting incoming coherent velocity data (from the LES) to outgoing Reynolds stress components (which are fed into, e.g., a dynamic subgrid scale model). The costly resolution of the near-wall region can thus be circumvented.

A more thorough analysis of the dynamic in-plane velocity-stress mapping and an assessment of its effectiveness in large-scale simulations will the topics of ongoing work.

Acknowledgments

The authors acknowledge the use of computational resources from the Certainty cluster awarded by the National Science Foundation to CTR. Fruitful discussions with Parviz Moin and with Beverley McKeon and her research group are gratefully acknowledged.

REFERENCES

Chen, K.K., Tu, J.H. & Rowley, C.W. 2012 Variants of dynamic mode decomposition: boundary condition, Koopman, and Fourier analyses. *J. Nonlinear Sci.* **22**, 887–915.

Jeong, J., Hussain, A.K.M.F., Schoppa, W. & Kim, J. 1997 Coherent structures near the wall in a turbulent channel flow. *J. Fluid Mech.* **332**, 185–214.

Jovanovic, M.R., Schmid, P.J. & Nichols, J.W. 2014 Sparsity-promoting dynamic mode decomposition. *Phys. Fluids* **26**, 024103.

Mezic, I. 2005 Spectral properties of dynamical systems, model reduction and decompositions. *Nonlinear Dynam.* **41**, 309–325.

Reynolds, W.C. & Hussain, A.K.M.F. 1972 The mechanics of an organized wave in turbulent shear flow. Part 3. Theoretical models and comparisons with experiments. *J. Fluid Mech.* **54**, 263–288.

Rowley, C.W., Mezic, I., Bagheri, S., Schlatter, P. & Henningson, D.S. 2009 Spectral analysis of nonlinear flows. *J. Fluid Mech.* **641**, 115–127.

Sayadi, T. 2012 *Numerical simulation of controlled transition to developed turbulence in a zero-pressure-gradient flat-plate boundary layer.* PhD Thesis, Stanford University.

Sayadi, T., Hamman, C.W. & Moin, P. 2013 Direct simulation of complete H-type and K-type transitions with implications for the structure of turbulent boundary layers. *J. Fluid Mech.* **724**, 480–509.

Sayadi, T. & Schmid, P.J. 2014 Reduced-order model for near-wall dynamics with implications for wall models. *Proceeding of the Summer Program*, Center for Turbulence Research, Stanford University, pp. 325-334.

Sayadi, T., Schmid, P.J., Nichols, J.W. & Moin, P. 2014 Reduced-order representation of near-wall structures in the late transitional boundary layer. *J. Fluid Mech.* **748**, 278–301.

Sayadi, T. & Schmid, P.J. 2016 Parallel data-driven decomposition algorithm for large-scale datasets: with application to transitional boundary layers. *Theor. Comp. Fluid Dyn.* **30**, 415-428.

Schmid, P.J. 2010 Dynamic mode decomposition of numerical and experimental data. *J. Fluid Mech.* **656** 5-28.

Schmid, P.J. & Sayadi, T. 2016 Low-dimensional representation of near-wall dynamics in shear flows, with implications to wall-models. *Phil. Trans. Roy. Soc. A* (in press).

Schmid, P.J., Violato, D. & Scarano, F. 2012 Decomposition of time-resolved tomographic PIV. *Exp. Fluids* **52**, 1567–1579.